

Exchange enhanced switching by alternating fields in quantum antiferromagnets

Asliddin Khudoyberdiev^{1,*} and Götz S. Uhrig^{1,†}

¹Condensed Matter Theory, TU Dortmund University,
Otto-Hahn-Straße 4, 44221 Dortmund, Germany

(Dated: July 2, 2024)

Information can be stored magnetically in antiferromagnets ultrafast since their characteristic times are on the picosecond scale. Various spin torques have proven to be important for efficient and high-speed magnetic memories. So far, this has been understood on the classical level by solving the equations of motion for macrospins describing the collective motion of the sublattice magnetizations. Since spins and hence magnetizations are deeply rooted in quantum mechanics, we show that the exchange enhanced manipulation of sublattice magnetizations extends to quantum antiferromagnets as well. To this end, we solve the time-dependent mean-field equations for Schwinger boson theory under external alternating magnetic fields. Exchange enhancement persists on the quantum level which includes dephasing effects. Significantly lower fields are sufficient to control the sublattice magnetization than for uniform fields which holds great promises for the realization of ultrafast magnetic storage devices.

One requirement for ultrafast storage devices is that they can be operated in the terahertz (THz) regime and that they provide a large storage capacity. Advancements in understanding and manipulating antiferromagnetic order paves the way for innovative technologies with disruptively improved performance. Antiferromagnets are promising candidates to speed up information processing because of their characteristic frequencies range in the THz regime [1]. Additionally, antiferromagnetic domains exhibit hardly any stray fields because their net magnetization cancels; this enables one to reduce the distance between domains encoding bits [2]. Nevertheless, the efficient control of antiferromagnetic order remains one of the main challenges for applications. In order to have bits robust against perturbations anisotropic spin systems are considered. In return, their manipulation requires to overcome activation energies [3, 4] for switching between the favored spin states [5, 6].

In the first place, efficient switching means that only low external fields need to be employed. In experimental and in classical macrospin descriptions it turned out [7–9] that it is advantageous to exploit so-called exchange enhancement. Since the internal fields exerted by adjacent spins via exchange coupling are by far larger than the external ones it is beneficial to have them assist in the reorientation of the Néel vector. This is achieved by slightly canting the antiparallel sublattice magnetizations so that a net magnetization is induced. Then, the sublattice magnetizations are precessing around the internal magnetic field stemming from the net magnetization, see Fig. 1.

At first sight, the required alternating magnetic field may appear elusive, but theoretical [10] and experimental progress [11, 12] in the last decade has shown that current-induced spin-orbit torques can be of Néel type,

i.e., they are alternating between the two sublattices. Recently, Behovits *et al.* [13] even achieved a deflection of the Néel vector in Mn₂Au by up to 30°. Besides current induced torques one can also conceive bipartite systems in which the \underline{g} tensor is anisotropic due to large spin-orbit couplings so that it is different $\underline{g}|_A \neq \underline{g}|_B$ between both sublattices. Then, even a uniform magnetic field \vec{B} of a THz pulse generates an alternating field $\vec{h}_a = (\underline{g}|_A - \underline{g}|_B)\mu_B\vec{B}/2$.

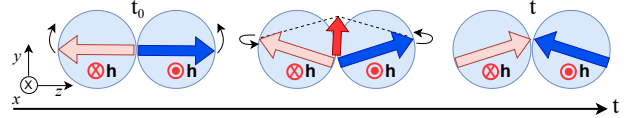


FIG. 1. Sketch of exchange enhanced switching by an alternating field. Light red and blue arrows stand for the magnetizations on sublattices A and B. The alternating external field \mathbf{h} tilts the magnetization in opposite directions so that a net magnetization is induced (dark red arrow) and thereby an internal exchange field around which both sublattice magnetizations quickly precess so that the Néel vector is essentially rotated by 180°. This illustration is a simplification because tilting and precessing happen simultaneously.

It is the present key objective to investigate the exchange enhanced control on the quantum level. We confirm that the characteristic energy is not h_a , but $\sqrt{Jh_a}$ where J is the exchange coupling [14–17]. This goal is achieved by using a time-dependent Schwinger mean-field theory which we have developed very recently [3, 4]. So far, it has been applied successfully to describe the effects of *uniform* static [3] and time-dependent external fields [4]. Its two main assets compared to classical macrospins are (i) to capture leading quantum fluctuations and (b) dephasing since all spin modes contribute at their respective frequencies [4]. The spin gap due to the spin anisotropy determines the required threshold field

* asliddin.khudoyberdiev@tu-dortmund.de

† goetz.uhrig@tu-dortmund.de

strength necessary to overcome the anisotropy potential barrier in reversing the orientation of the sublattice magnetization. The switching time, i.e., the time required to achieve the reorientation is inversely proportional to the external uniform field, i.e., $t^{\text{sw}} \propto 1/h$. Here, we extend this analysis to the relevant case of alternating fields. The particularly promising finding is that much smaller fields are sufficient for switching and that the switching dynamics is still ultrafast.

Concretely, we consider the easy-axis spin-1/2 Heisenberg model at zero temperature on a simple cubic lattice[18] with nearest-neighbor interactions

$$\mathcal{H}_0 = J \sum_{\langle i,j \rangle} \left\{ \frac{\chi}{2} (S_i^+ S_j^- + S_i^- S_j^+) + S_i^z S_j^z \right\}, \quad (1)$$

where $J_x = J_y = J_{xy}$, $J_z = J$ and $\chi = J_{xy}/J_z$. The Zeeman term for an alternating time-dependent magnetic field reads

$$\mathcal{H}_{\text{alt}} = -\vec{h}_a(t) \cdot \sum_i (-1)^i \vec{S}_i. \quad (2)$$

For technical reason, we specify \vec{h}_a to point along the x axis. We use J as energy unit.

Standard spin wave theory according to Holstein-Primakoff or Dyson-Maleev only expands in fluctuations around the ordered state which is not appropriate for capturing reorientations by 180° . Thus, we employ the the Schwinger boson representation

$$S_i^+ = a_i^\dagger b_i, \quad S_i^- = b_i^\dagger a_i, \quad S_i^z = \frac{1}{2} (a_i^\dagger a_i - b_i^\dagger b_i) \quad (3)$$

with two bosons per site and the constraint $2S = a_i^\dagger a_i + b_i^\dagger b_i$ which is fulfilled on average in the mean-field approach [19, 20]. The sublattice magnetization in z direction reads

$$m = \frac{1}{2} (\langle a_i^\dagger a_i \rangle - \langle b_i^\dagger b_i \rangle). \quad (4)$$

All equations simplify by a sublattice rotation as it is common for antiferromagnets. We rotate all spins on the B lattice by 180° about S_i^y which implies for the Schwinger bosons $a_j \rightarrow -b_j$ and $b_j \rightarrow a_j$. Since this results $S^x \rightarrow -S^x$ on sublattice B, the alternating external field in x direction becomes uniform [21] so that the Hamiltonian after the sublattice rotation is translationally invariant and reads

$$\mathcal{H} = J \sum_{\langle i,j \rangle} \left\{ \frac{\chi}{2} (S_i^+ S_j^+ + S_i^- S_j^-) + S_i^z S_j^z \right\} - h_a(t) \sum_i S_i^x. \quad (5)$$

This is re-expressed in Schwinger bosons according to (3). The mean-field Hamiltonian is obtained by introducing the complex expectation values $A := \langle a_i a_j + b_i b_j \rangle$ and $B := \langle a_i a_j - b_i b_j \rangle$ and applying Wick's theorem. After

Fourier transformation the bilinear mean-field Hamiltonian reads

$$\begin{aligned} \mathcal{H}_{\text{MF}} = E_0 - \frac{z}{8} \sum_{\mathbf{k}} \gamma_{\mathbf{k}} (C_- a_{-\mathbf{k}}^\dagger a_{-\mathbf{k}}^\dagger + C_+ b_{\mathbf{k}}^\dagger b_{-\mathbf{k}}^\dagger \\ + C_-^* a_{\mathbf{k}} a_{-\mathbf{k}} + C_+^* b_{\mathbf{k}} b_{-\mathbf{k}}) + \lambda \sum_{\mathbf{k}} (a_{\mathbf{k}}^\dagger a_{\mathbf{k}} + b_{\mathbf{k}}^\dagger b_{\mathbf{k}}) \\ - \frac{1}{2} h_a(t) \sum_{\mathbf{k}} (a_{\mathbf{k}}^\dagger b_{\mathbf{k}} + b_{\mathbf{k}}^\dagger a_{\mathbf{k}}), \end{aligned} \quad (6)$$

where z is the coordination number and $C_\pm := A(1 + \chi) \mp B(1 - \chi)$. The energy E_0 does not contribute to the dynamics of the system so that we omit it henceforth. The wave vector only enters via

$$\gamma_{\mathbf{k}} = \frac{1}{d} \sum_{i=1}^d \cos k_i, \quad (7)$$

where d is dimension of the lattice and the lattice constant is set to unity.

The initial conditions are found by Bogoliubov transformation of the boson and self-consistently determination of A , B , and other expectation values, see Refs. [3, 19, 20]. We follow this route as well, but finally transform the results back to the expectation values $\langle a_{\mathbf{k}} a_{-\mathbf{k}} \rangle$, $\langle b_{\mathbf{k}} b_{-\mathbf{k}} \rangle$ and of their conjugates as well as of $\langle a_{\mathbf{k}}^\dagger a_{\mathbf{k}} \rangle$ and $\langle b_{\mathbf{k}}^\dagger b_{\mathbf{k}} \rangle$, see Supplement [22]. Since only $\gamma_{\mathbf{k}}$ matters, it is sufficient to discretize the interval $\gamma \in [-1, 1]$ and to determine for the discrete values $\langle a_{\mathbf{k}} a_{-\mathbf{k}} \rangle_\gamma$, $\langle b_{\mathbf{k}} b_{-\mathbf{k}} \rangle_\gamma$, $\langle a_{\mathbf{k}}^\dagger a_{\mathbf{k}} \rangle_\gamma$ and $\langle b_{\mathbf{k}}^\dagger b_{\mathbf{k}} \rangle_\gamma$. This simplifies the numerics greatly and makes high-precision computations in three dimension possible; the required densities-of-states are given in the Supplement [22] where the Heisenberg equations of motions resulting from the mean-field Hamiltonian \mathcal{H}_{MF} are also provided.

Control is achieved by an external magnetic field. This can be done by a static, constant field h_{static} or by a pulse of finite duration and maximum amplitude h_{pulse} . We study both variants, but expect from previous results [3, 4] that pulses are more efficient if the pulse frequency is close to resonance with the spin gap. THz pulses are advantageous anyway in view of experimental feasibility [23]. We consider the alternating pulse (subscript 'a')

$$h_a(t) = h_{\text{a,pulse}} \cos(\alpha \Delta (t - 3\tau) + \phi_0) \cdot e^{-\frac{(t-3\tau)^2}{2\tau^2}} \quad (8)$$

where $h_{\text{a,pulse}}$ is the maximum amplitude, Δ is the spin gap, $\alpha < 1$ is a renormalization factor to optimize the resonance, and ϕ_0 is a phase shift. The pulse duration is given by τ . Since we start the simulations at $t = 0$ we shift the pulse by 3τ to capture it fully. The analysis and optimization of the pulse parameters in (8) are given in Supplemental Material [22]. It turns out that the same parameters as for uniform fields [4] yield good results. Hence we use again $\alpha = 0.85$, $\tau = 10 J^{-1}$, and $\phi_0 = \pi/3$.

Figure 2 displays two representative behaviors of the sublattice magnetization subject to pulses of the type

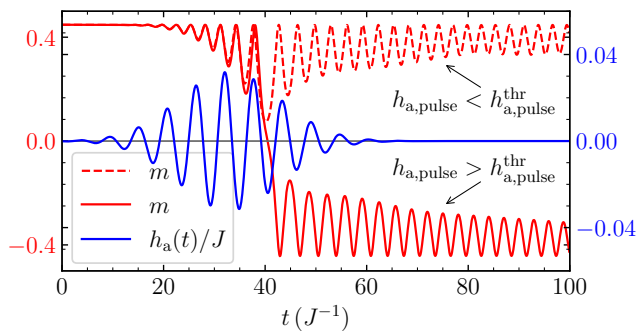


FIG. 2. Evolution of the sublattice magnetization $m(t)$ for $h_{a,\text{pulse}} = 0.031 J$ (dashed red line) and $h_{a,\text{pulse}} = 0.032 J$ (solid red line) at $\chi = 0.9$ where $h_{a,\text{pulse}}^{\text{thr}} = 0.0313 J$. The values of the pulse with $h_{a,\text{pulse}} = 0.032 J$ (blue line) are denoted on the right y axis.

(8). There is a threshold value of the amplitude which has to be overcome to realize switching that is clearly signaled by the sign change of $m(t)$. If the pulse has too low amplitude only oscillations close to the initial magnetization are induced. A large enough amplitude nudges the magnetization over its anisotropic maximum so that it oscillates thereafter close to its negative equilibrium value. The oscillations as such are not surprising since the pulse perturbs the system injecting energy so that oscillations are induced. We emphasize that no relaxation is included here since we want to study the closed quantum system. In view of the absence of relaxation one may wonder why the oscillations decrease at all. Indeed, typical classical macrospin calculations without relaxation display persisting sign changes; no decrease in oscillations is observed [4]. The observed decrease in the quantum model results from dephasing. Many modes contribute to collective observables such as $m(t)$ with their individual frequencies so that the increasing phase differences lead to a decreasing total signal. This is clearly visible in Fig. 2 and was to be expected from previous quantum calculations [3, 4]. Relaxation will surely speed up the decrease of the oscillations. But its quantitative investigation is beyond the scope of the present study. Here, we conclude that the applied amplitude of the pulse is sufficiently low to reach the realizable range, e.g., $h_{0a} = 0.032 J$ correspond to about 2.8 T for antiferromagnetic coupling constant $J = 10$ meV. The threshold value decreases further for weaker anisotropy $\chi \rightarrow 1$.

Figure 3 depicts our key result. The threshold values labeled by the superscript $^{\text{thr}}$ for the four variants considered are plotted. The corresponding amplitudes are $h_{u,\text{static}}$ for a uniform, constant field, $h_{u,\text{pulse}}$ for a uniform pulse, $h_{a,\text{static}}$ for an alternating, constant field, and $h_{a,\text{pulse}}$ for an alternating pulse. The crucial observation is the very different power law behavior for $\chi \rightarrow 1$. For uniform, static field we had established that the threshold is almost quantitatively given by the spin gap implying $h^{\text{thr}} \propto \sqrt{1 - \chi}$, see orange line in Fig. 3. Such a sublin-

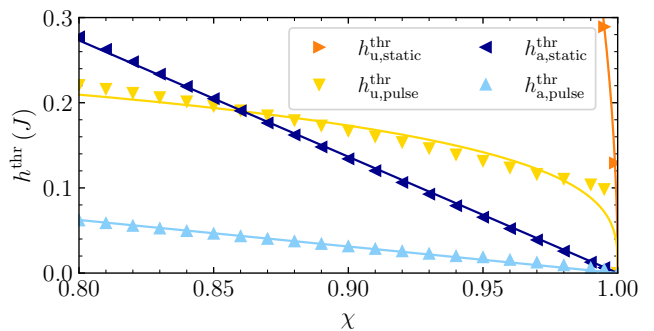


FIG. 3. Threshold fields vs. anisotropy χ for the simple cubic lattice. The fits (solid lines) for uniform fields use $h_u^{\text{thr}} = c_u(1 - \chi^2)^n$ where for static case we find $c_u \approx 2.96 J$, $n \approx 0.504 \pm 0.585$ and for the pulse $c_u \approx 0.28 J$, $n = 0.30 \pm 0.02$. For alternating fields, the behavior is clearly linear which we fit by $h_a^{\text{thr}} = c_a(1 - \chi)$, where $c_a \approx 1.365 J$ for the static and $c_a \approx 0.312 J$ for the time-dependent case.

ear power law is also indicated by the results given by the yellow line. The uniform static case requires by far the largest fields. The alternating static and pulse case display linear behavior which implies the highly advantageous feature that their thresholds become much smaller than the uniform ones for weak anisotropies $\chi \rightarrow 1$. This is a direct consequence of the exchange enhancement. The activation energy to overcome is given by the spin gap $\Delta \propto \sqrt{1 - \chi}$. If the relevant energy scale of the control field is $\sqrt{Jh_a}$ instead of h_a the ensuing threshold is linear in $1 - \chi$

$$\Delta \propto J\sqrt{1 - \chi} \propto \sqrt{Jh_a^{\text{thr}}} \Rightarrow h_a^{\text{thr}} \propto J(1 - \chi). \quad (9)$$

For an estimate, the threshold at $\chi = 0.995$ is $h_{a,\text{pulse}}^{\text{thr}} = 0.0041 J$ corresponding to about 0.5 T only at $J \approx 14$ meV. These observations in a quantum model show strikingly the advantages of using alternating pulses for the re-orientation of magnetizations.

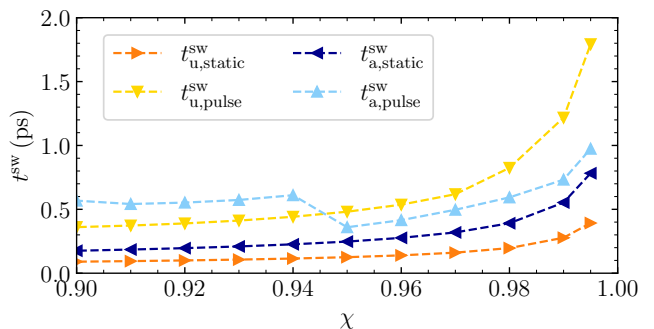


FIG. 4. Switching time vs. the anisotropy for fields 20% above the values shown in Fig. 3. For the pulses, we measure t^{sw} not from $t = 0$, but from the center of the pulse, i.e., we deduct 3τ .

The next key quantity to study is the switching time,

i.e., the time required for the manipulation. Low switching fields which in turn lead to very long switching times t^{sw} would not be of great help in view of applications. Thus, we analyze the time it takes for the relevant sign change in $m(t)$ to occur if we switch the system with an amplitude 20% above the threshold. Using this increased values is numerically more stable than a study at the marginal field amplitude. In any application one would surely use sufficiently large fields for the control. Figure 4 shows the switching time as a function of the anisotropy. For concreteness, we provide times in picoseconds assuming an exchange coupling of $J \approx 10\text{meV}$. At first glance, Fig. 4 does not convey a clear message because the pulses take longer than the static fields and the quickest switch is not obtained by the alternating field, but by the uniform one. But one has to keep in mind that the employed control fields are very different, namely much smaller for the pulses than for the static fields. Hence, the message from Fig. 4 is not the difference between the different variants, but their similarity: despite the largely different fields the switching times are in the range of ≈ 1 ps. This confirms that the THz range is the appropriate range of magnetization re-orientation in quantum antiferromagnets.

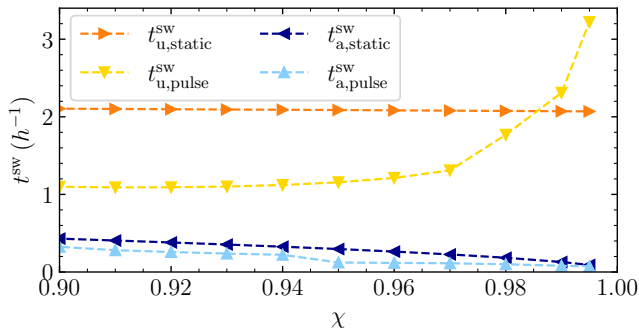


FIG. 5. Switching times of the four variants expressed relative to the applied field amplitude $h = 1.2h^{\text{thr}}$.

To underline that the switching speed must be seen relative to the employed field amplitudes we plot the data from Fig. 4 in Fig. 5 in units of $1/h$ [3]. This rendering clearly shows that the alternating fields are more efficient than the uniform ones. Also, the pulses are advantageous relative to constant fields. For the uniform, static case an almost constant result is observed implying that for sufficiently large fields only the field amplitude determines the dynamics. For the uniform pulse, we find indications of a weak divergence of the switching time showing that the some power of the inverse spin gap determines t^{sw} . This is qualitatively consistent with the weak decrease of $h_{\text{u,pulse}}^{\text{thr}}$ we observed in Fig. 4. The two blue lines corresponding to the alternating fields show decreasing values of ht^{sw} for χ tending to 1 which reflects a proportionality $\propto \sqrt{1-\chi}$. This is understood from the estimate

$$h_a^{\text{thr}} t_a^{\text{sw}} \propto \frac{J(1-\chi)}{\sqrt{Jh^{\text{thr}}}} \propto \frac{J(1-\chi)}{\Delta} \propto \sqrt{1-\chi}. \quad (10)$$

Hence, it is not surprising that the alternating control field provides the fastest control in spite of using the smallest control fields. This is a very promising observation in view of experimental realizations.

On the way to using magnetic degrees of freedom for data storage and handling antiferromagnetism is a realm to be fully understood, in particular the possibilities of control by external fields. This is required for writing and erasing data. We investigated the effect of alternating control fields on the orientation of the sublattice magnetization in an easy-axis Heisenberg quantum antiferromagnet on a simple cubic lattice with numerical results for $S = 1/2$. The fields alternate in orientation between the two sublattice and they are assumed to be static or in pulse shape with a carrier frequency of slightly below resonance to the spin gap. The employed tool was time-dependent Schwinger boson mean-field theory because it is the only mean-field approach able to describe full revolutions in time of the magnetic order as well as the static equilibrium while maintaining the assets of a quantum model.

In line with previous classical and experimental evidence, our results clearly show that alternating effective magnetic fields, also called Néel spin torques, are the best choice for a rapid manipulation of the expectation value of the sublattice magnetization. Much lower fields are needed than for uniform fields because of the exchange enhancement which implies that the characteristic energy of the control field is not h , but \sqrt{Jh} where $h = g\mu_B B$. Very importantly, also the time required for performing the manipulation does not grow too much. Even for very weak fields we predict a switching time in the picosecond range. The required fields can be as low as tenths of Tesla. For $\chi = 0.999$, we estimate $h_{\text{a,pulse}}^{\text{thr}} = 0.0021 J$; this corresponds roughly to ≈ 0.2 Tesla assuming $J \approx 10\text{meV}$ for the simple cubic lattice. In summary, these results and the method developed to obtain them pave the way to a better understanding of magnetization dynamics and hence a sustainable information processing based on quantum antiferromagnetism.

Next steps of a theoretical analysis suggesting themselves are the inclusion of relaxation on the quantum level [24]. The spin size S can very easily be enhanced which in turn allows to consider more complex anisotropies, for instance with four-fold equilibrium orientations of the magnetization. Finally, other bipartite lattice can be addressed as well in a quite straightforward manner. Hence, there is a plethora of systems and issues to be studied in the near future.

We are grateful for helpful discussion with Tobias Kampfrath. This work has been financially supported by the Deutsche Forschungsgemeinschaft (German Research Foundation) in project UH 90/14-1 and by the Stiftung Mercator in project Ko-2021-0027.

- [1] T. Jungwirth, X. Marti, P. Wadley, and J. Wunderlich, Antiferromagnetic spintronics, *Nature Nanotechnology* **11**, 231 (2016).
- [2] S. Loth, S. Baumann, C. P. Lutz, D. M. Eigler, and A. J. Heinrich, Bistability in atomic-scale antiferromagnets, *Science* **335**, 196 (2012).
- [3] K. Bolsmann, A. Khudoyberdiev, and G. S. Uhrig, Switching the magnetization in quantum antiferromagnets, *PRX Quantum* **4**, 030332 (2023).
- [4] A. Khudoyberdiev and G. S. Uhrig, Switching of magnetization in quantum antiferromagnets with time-dependent control fields, *Physical Review B* **109**, 174419 (2024).
- [5] O. Gomonay, T. Jungwirth, and J. Sinova, Concepts of antiferromagnetic spintronics, *Physica Status Solidi - Rapid Research Letters* **11**, 1700022 (2017).
- [6] C. Song, Y. You, X. Chen, X. Zhou, Y. Wang, and F. Pan, How to manipulate magnetic states of antiferromagnets, *Nanotechnology* **29**, 112001 (2018).
- [7] H. V. Gomonay and V. M. Loktev, Spin transfer and current-induced switching in antiferromagnets, *Physical Review B* **81**, 144427 (2010).
- [8] P. Wadley, B. Howells, J. Železný, C. Andrews, V. Hills, R. P. Campion, V. Novák, K. Olejník, F. Maccherozzi, S. S. Dhesi, S. Y. Martin, T. Wagner, J. Wunderlich, F. Freimuth, Y. Mokrousov, J. Kuneš, J. S. Chauhan, M. J. Grzybowski, A. W. Rushforth, K. W. Edmonds, B. L. Gallagher, and T. Jungwirth, Electrical switching of an antiferromagnet, *Science* **351**, 587 (2016).
- [9] P. E. Roy, R. M. Otxoa, and J. Wunderlich, Robust picosecond writing of a layered antiferromagnet by staggered spin-orbit fields, *Physical Review B* **94**, 014439 (2016).
- [10] J. Železný, H. Gao, K. Výborný, J. Zemen, J. Mašek, A. Manchon, J. Wunderlich, J. Sinova, and T. Jungwirth, Relativistic Néel-Order Fields Induced by Electrical Current in Antiferromagnets, *Physical Review Letters* **113**, 157201 (2014).
- [11] K. Olejník, T. Seifert, Z. Kašpar, V. Novák, P. Wadley, R. P. Campion, M. Baumgartner, P. Gambardella, P. Němec, J. Wunderlich, J. Sinova, P. Kužel, M. Müller, T. Kampfrath, and T. Jungwirth, Terahertz electrical writing speed in an antiferromagnetic memory, *Science Advances* **4**, eaar3566 (2018).
- [12] S. Y. Bodnar, L. Šmejkal, I. Turek, T. Jungwirth, O. Gomonay, J. Sinova, A. A. Sapozhnik, H.-J. Elmers, M. Kläui, and M. Jourdan, Writing and reading antiferromagnetic mn_2Au by nél spin-orbit torques and large anisotropic magnetoresistance, *Nature Communications* **9**, 348 (2018).
- [13] Y. Behovits, A. L. Chekhov, S. Y. Bodnar, O. Gueckstock, S. Reimers, Y. Lytvynenko, Y. Skourski, M. Wolf, T. S. Seifert, O. Gomonay, M. Kläui, M. Jourdan, and T. Kampfrath, Terahertz Néel spin-orbit torques drive nonlinear magnon dynamics in antiferromagnetic Mn_2Au , *Nature Communications* **14**, 6038 (2023).
- [14] C. Kittel, Theory of antiferromagnetic resonance, *Phys. Rev.* **82**, 565 (1951).
- [15] A. V. Kimel, A. Kirilyuk, A. Tsvetkov, R. V. Pisarev, and T. Rasing, Laser-induced ultrafast spin reorientation in the antiferromagnet TmFeO_3 , *Nature* **429**, 850 (2004).
- [16] O. Gomonay, T. Jungwirth, and J. Sinova, High Antiferromagnetic Domain Wall Velocity Induced by Néel Spin-Orbit Torques, *Physical Review Letters* **117**, 017202 (2016).
- [17] O. Gomonay, T. Jungwirth, and J. Sinova, Narrow-band tunable terahertz detector in antiferromagnets via staggered-field and antidamping torques, *Physical Review B* **98**, 104430 (2018).
- [18] Results for the square lattice are included in the Supplemental Material [22].
- [19] A. Auerbach and D. P. Arovas, Spin dynamics in the square-lattice antiferromagnet, *Physical Review Letters* **61**, 617 (1988).
- [20] A. Auerbach, *Interacting Electrons and Quantum Magnetism*, Graduate Texts in Contemporary Physics (Springer, New York, 1994).
- [21] A uniform control field is realized by applying the field in y direction [3, 4].
- [22] xx, See supplemental material, NA **1**, 1 (1111).
- [23] T. Kampfrath, A. Sell, G. Klatt, A. Pashkin, S. Mährlein, T. Dekorsy, M. Wolf, M. Fiebig, A. Leitenstorfer, and R. Huber, Coherent terahertz control of antiferromagnetic spin waves, *Nature Photonics* **5**, 31 (2011).
- [24] G. S. Uhrig, Landau-Lifshitz damping from Lindbladian dissipation in quantum magnets, arXiv: **2406.10613** (2024).
- [25] T. Hanisch, G. S. Uhrig, and E. Müller-Hartmann, Lattice dependence of saturated ferromagnetism in the Hubbard model, *Physical Review B* **56**, 13960 (1997).
- [26] S. Miyashita and B. Barbara, How to cross an energy barrier at zero kelvin without tunneling effect, *Physical Review Letters* **131**, 066701 (2023).

I. SUPPLEMENTAL MATERIAL

A. Calculation of density-of-states of γ_k

To consider long range order in the system, it is important to choose the lattice size large enough. However, possible points in Brillouin zone becomes large especially for 3D simple cubic lattice and the sums in the Hamiltonian in momentum space will be numerically unmanageable. Hence, instead of summing over each value of momentum in first Brillouin zone, one can convert the sums into one dimensional integrals as

$$\lim_{N \rightarrow \infty} \frac{1}{N} \sum_k F(\gamma_k) = \int_{-1}^1 d\gamma \rho(\gamma) F(\gamma) \quad (11)$$

where $\rho(\gamma)$ is density of state in d dimension. It has the following forms for square and simple cubic lattices [25]

$$\rho_{\text{sq}}(\gamma) = \frac{2}{\pi^2} K(1 - \gamma^2), \quad (12a)$$

$$\rho_{\text{cub}}(\gamma) = \frac{1}{\pi} \int_{u_1}^{u_2} \frac{du}{\sqrt{1 - u^2}} \rho_{\text{sq}}(\gamma + u/3), \quad (12b)$$

$$u_1 = \max(-1, -2 - 3\gamma), \quad u_2 = \min(1, 2 - 3\gamma). \quad (12c)$$

We calculated these integrals with Newton-Cotes mid-point interval rule. Now, to calculate the integral in (11), one can discretize it for possible γ points and solve differential equations, obtained from Heisenberg's equation motion in the main text, for each values of γ where $\gamma \in [-1, 1]$. We have chosen 2000 gamma points in the given interval and the results are consistent with sum method for sufficiently large lattice size.

B. Equations for the non-equilibrium dynamics of expectation values

The mean-occupation numbers of a and b bosons can be calculated in the equilibrium within the process of Hamiltonian diagonalization

$$\langle a_{\mathbf{k}}^\dagger a_{\mathbf{k}} \rangle_\gamma = \frac{\lambda}{2\omega_k^-(\gamma)} - \frac{1}{2}, \quad (13a)$$

$$\langle b_{\mathbf{k}}^\dagger b_{\mathbf{k}} \rangle_\gamma = \frac{\lambda}{2\omega_k^+(\gamma)} - \frac{1}{2}. \quad (13b)$$

Here, the spin wave dispersion relations for α and β bosons ω_k^- and ω_k^+ , respectively, reads

$$\omega_k^\pm = \sqrt{\lambda^2 - (z|C_\pm|\gamma_k/4)^2}. \quad (14)$$

Due to the anisotropy, both boson dispersions gain an energy gap as

$$\Delta^\pm := \omega_{\mathbf{k}=0}^\pm. \quad \Delta = \Delta^+ - \Delta^-, \quad (15)$$

where Δ is the physical spin gap.

The variables A and B required to compute C_\pm in (6) are defined by

$$A = \langle a_i a_j \rangle + \langle b_i b_j \rangle \quad (16a)$$

$$= \int_{-1}^1 \gamma \rho_d(\gamma) (\langle a_{\mathbf{k}} a_{-\mathbf{k}} \rangle_\gamma + \langle b_{\mathbf{k}} b_{-\mathbf{k}} \rangle_\gamma) d\gamma, \quad (16b)$$

$$B = \langle a_i a_j \rangle - \langle b_i b_j \rangle \quad (16c)$$

$$= \int_{-1}^1 \gamma \rho_d(\gamma) (\langle a_{\mathbf{k}} a_{-\mathbf{k}} \rangle_\gamma - \langle b_{\mathbf{k}} b_{-\mathbf{k}} \rangle_\gamma) d\gamma, \quad (16d)$$

$$2S = \langle a_i^\dagger a_i \rangle + \langle b_i^\dagger b_i \rangle \quad (16e)$$

$$= \int_{-1}^1 \rho_d(\gamma) (\langle a_{\mathbf{k}}^\dagger a_{\mathbf{k}} \rangle_\gamma + \langle b_{\mathbf{k}}^\dagger b_{\mathbf{k}} \rangle_\gamma) d\gamma. \quad (16f)$$

The last equation responsible to fulfill the constraints on boson number and the density $\rho_d(\gamma)$ is the density-of-states in d dimensions for $\gamma_{\mathbf{k}}$ [25]. The other expectation values are

$$\langle a_{\mathbf{k}} a_{-\mathbf{k}} \rangle_\gamma = \frac{z\gamma C_-}{8\omega_k^-(\gamma)}, \quad (17a)$$

$$\langle b_{\mathbf{k}} b_{-\mathbf{k}} \rangle_\gamma = \frac{z\gamma C_+}{8\omega_k^+(\gamma)}. \quad (17b)$$

Finally, the temporal evolution is determined from the equations of motion for the introduced expectation values. As stated before, this dynamics only depends on the value $\gamma_{\mathbf{k}} = \gamma$

$$\begin{aligned} \partial_t \langle a_{\mathbf{k}}^\dagger a_{\mathbf{k}} \rangle_\gamma &= -i\frac{z}{4}\gamma (C_-^* \langle a_{\mathbf{k}} a_{-\mathbf{k}} \rangle_\gamma - C_- \langle a_{\mathbf{k}}^\dagger a_{-\mathbf{k}}^\dagger \rangle_\gamma) \\ &\quad + i\frac{h_x}{2} (\langle a_{\mathbf{k}}^\dagger b_{\mathbf{k}} \rangle_\gamma - \langle b_{\mathbf{k}}^\dagger a_{\mathbf{k}} \rangle_\gamma), \end{aligned} \quad (18a)$$

$$\begin{aligned} \partial_t \langle b_{\mathbf{k}}^\dagger b_{\mathbf{k}} \rangle_\gamma &= -i\frac{z}{4}\gamma (C_+^* \langle b_{\mathbf{k}} b_{-\mathbf{k}} \rangle_\gamma - C_+ \langle b_{\mathbf{k}}^\dagger b_{-\mathbf{k}}^\dagger \rangle_\gamma) \\ &\quad - i\frac{h_x}{2} (\langle a_{\mathbf{k}}^\dagger b_{\mathbf{k}} \rangle_\gamma - \langle b_{\mathbf{k}}^\dagger a_{\mathbf{k}} \rangle_\gamma), \end{aligned} \quad (18b)$$

$$\begin{aligned} \partial_t \langle a_{\mathbf{k}} a_{-\mathbf{k}} \rangle_\gamma &= i\frac{z}{4}\gamma [C_- (2\langle a_{\mathbf{k}}^\dagger a_{\mathbf{k}} \rangle_\gamma + 1)] \\ &\quad - 2\lambda i \langle a_{\mathbf{k}} a_{-\mathbf{k}} \rangle_\gamma + i h_x \langle a_{\mathbf{k}} b_{-\mathbf{k}} \rangle_\gamma, \end{aligned} \quad (18c)$$

$$\begin{aligned} \partial_t \langle b_{\mathbf{k}} b_{-\mathbf{k}} \rangle_\gamma &= i\frac{z}{4}\gamma [C_+ (2\langle b_{\mathbf{k}}^\dagger b_{\mathbf{k}} \rangle_\gamma + 1)] \\ &\quad - 2\lambda i \langle b_{\mathbf{k}} b_{-\mathbf{k}} \rangle_\gamma + i h_x \langle a_{\mathbf{k}} b_{-\mathbf{k}} \rangle_\gamma, \end{aligned} \quad (18d)$$

$$\begin{aligned} \partial_t \langle a_{\mathbf{k}}^\dagger b_{\mathbf{k}} \rangle_\gamma &= -i\frac{z}{4}\gamma (C_-^* \langle a_{\mathbf{k}} b_{-\mathbf{k}} \rangle_\gamma - C_+ \langle a_{\mathbf{k}}^\dagger b_{-\mathbf{k}}^\dagger \rangle_\gamma) \\ &\quad - i\frac{h_x}{2} (\langle b_{\mathbf{k}}^\dagger b_{\mathbf{k}} \rangle_\gamma - \langle a_{\mathbf{k}}^\dagger a_{\mathbf{k}} \rangle_\gamma), \end{aligned} \quad (18e)$$

$$\begin{aligned} \partial_t \langle a_{\mathbf{k}} b_{-\mathbf{k}} \rangle_\gamma &= i\frac{z}{4}\gamma (C_- \langle a_{\mathbf{k}}^\dagger b_{\mathbf{k}} \rangle_\gamma + C_+ \langle b_{\mathbf{k}}^\dagger a_{\mathbf{k}} \rangle_\gamma) \\ &\quad - 2\lambda i \langle a_{\mathbf{k}} b_{-\mathbf{k}} \rangle_\gamma \\ &\quad + i\frac{h_x}{2} (\langle a_{\mathbf{k}} a_{-\mathbf{k}} \rangle_\gamma + \langle b_{\mathbf{k}} b_{-\mathbf{k}} \rangle_\gamma). \end{aligned} \quad (18f)$$

These above set of differential equations are solved with calculated initial values from (13) and (17).

C. The analyses of the pulse for a simple cubic lattice

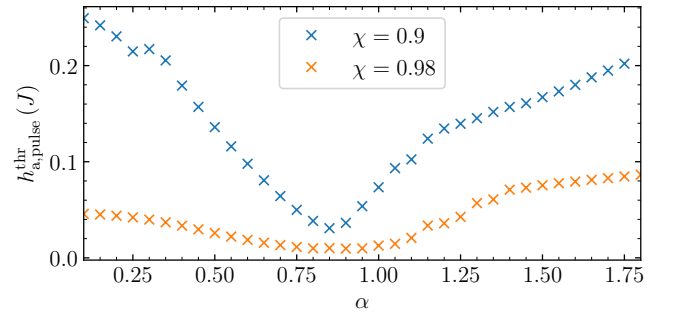


FIG. 6. Threshold field dependence on frequency renormalization constant in (8). The other parameters are $\phi_0 = \pi/3$ and $\tau = 10 J^{-1}$.

Figure 6 shows the essence of the resonance where $h_{a,\text{static}}^{\text{thr}}$ is the threshold amplitude of the pulse in Eq. (8) to switch antiferromagnetic order. The perturbation energy should be in the order of spin gap Δ . In particular, slight deviation from the frequency $\omega = \Delta$ occurs and the anisotropy gap decreases around switching process

due to different level separations between the states [26]. Hence, frequency renormalization constant α is helpful to catch the best resonance coupling. According to our test results, $\alpha \approx 0.85$ is the optimum value for valid χ with lowest threshold field as in Ref. [4]. The overall dependence is not exactly parabolic because of ultrafast dynamics and quite strong quantum fluctuations under very strong effective fields in the regions away from optimal values of α .

The initial phase of the pulse also crucial to catch proper spin dynamics at best resonance. For this reason we analyzed its effect on switching. Fig. 7 illustrates the threshold amplitude of the pulse dependence on initial phase. Although the dependence is very weak, the unexpected jumps also occur in this case as it was obtained recently [4]. These jumps are the results of shift in switching time at some preferred oscillation under the pulse. Based on fully analyses of the pulse for other anisotropy parameters considering square lattice as well, we have chosen $\phi_0 = \pi/3$ as an optimum value.

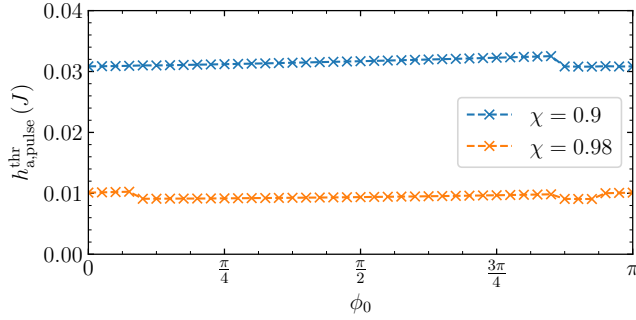


FIG. 7. Threshold field dependence on initial phase with $\alpha = 0.85$ and $\tau = 10 J^{-1}$.

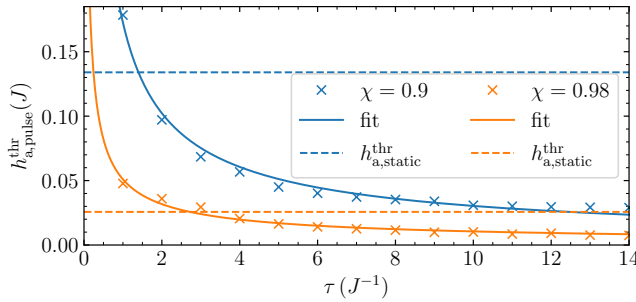


FIG. 8. Threshold field dependence on pulse duration with $\alpha = 0.85$ and $\phi_0 = \pi/3$. Dashed horizontal lines correspond to the threshold values for alternating static magnetic field with $h_{a,static}^{thr} = 0.134 J$ and $h_{a,static}^{thr} = 0.0257 J$ for $\chi = 0.9$ and $\chi = 0.98$, respectively. The fits (solid lines) are done by power laws $h_{a,pulse}^{thr} = a\tau^b$ with parameters $a = 0.172 J^{b+1}$, $b = -0.755$ for $\chi = 0.9$ and $a = 0.05 J^{b+1}$, $b = -0.684$ for $\chi = 0.98$.

Finally, the threshold field dependence on pulse duration is analyzed in Fig. 8. Obviously, longer pulses result

switching at lower fields but its effect is not strong after $\tau > 10 J^{-1}$. The fittings are done by the power law $h_{a,pulse}^{thr} = a\tau^b$ and the fitting parameters a and b are indicated in the caption. The power law shows that the long lasting pulses can decrease the threshold values even to very small minimum as τ goes to infinity. However, we have limited the duration with $\tau = 10 J^{-1}$ being the optimal value for our realistic pulse.

D. Switching in square lattice by alternating fields

Here, we represent results for 2D square lattice under static and time-dependent alternating fields. General physics behind is similar to the 3D case but with lower threshold fields as the spin gap is lower in 2D case.

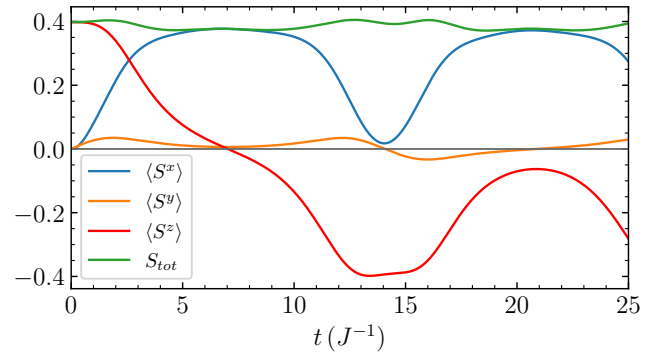


FIG. 9. The dynamics of spin expectation values for $h_{a,static} = 0.08 J > h_{a,static}^{thr}$ and $\chi = 0.9$. The modules of total spin expectation value is given by $S_{tot} = \sqrt{\langle S^x \rangle^2 + \langle S^y \rangle^2 + \langle S^z \rangle^2}$.

Firstly, the dynamics of spin expectation values is shown in Fig. 9. Overall dynamics justify the switching process in our illustration in the main part (see Fig. 1) with Larmor oscillations about x axis and very small canting of $\langle S^y \rangle$. Clearly, the quantum oscillations also occur in the modules of total spin expectation value.

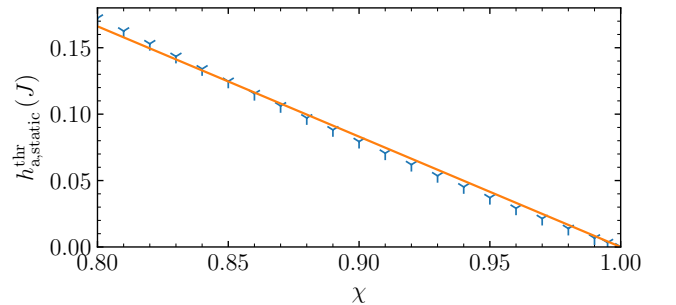


FIG. 10. Threshold field dependence on anisotropy parameter. The fitting is done by $h_{a,static}^{thr} = c(1 - \chi)$ where $c = 0.831 J$.

Figure 10 shows threshold field dependence on anisotropy parameter in complete analogy with the 3D

case. The last minimum value correspond to the $\chi = 0.995$ with $h_{a,\text{static}}^{\text{thr}} = 0.0032 J$. This field is approximately 0.3 Tesla if one considers an appropriate antiferromagnetic exchange interaction constant. Hence, our quantum approach claims that the switching antiferromagnetic order is possible with quite low alternating fields.

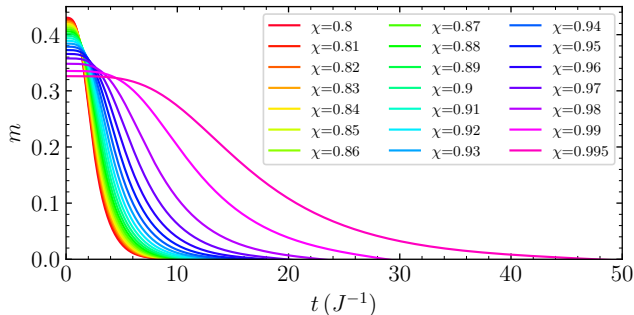


FIG. 11. Dynamics of sublattice magnetization at threshold values of alternating, static fields.

The dynamics of sublattice magnetization under threshold alternating static field is given in Fig. 11 for different anisotropies. One can clearly see that the weak anisotropies result slower dynamics with switching at later times, but still in THz range.

The calculated switching time versus anisotropy are shown in Fig. 12. When the switching field increased by a factor of 1.1 or 1.5, we obtain earlier time switching and switching time controlled by the anisotropy of the system with inversely square root behaviour. Indeed, this is in agreement with $\sqrt{Jh_a}$ energy scale as h_a has linear dependence on χ .

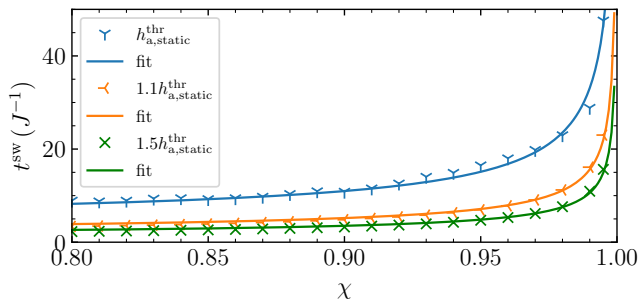


FIG. 12. Switching time dependence on anisotropy. The fits are by $t^{sw} = c/\sqrt{1-\chi}$ where $c = 3.294$ for $h_{a,\text{static}}^{\text{thr}}$, $c = 1.553$ for $1.1h_{a,\text{static}}^{\text{thr}}$ and $c = 1.054$ for $1.5h_{a,\text{static}}^{\text{thr}}$.

Next, we compare the switching time of sublattice magnetization under uniform and alternating external static fields. According to the calculations in both fields with 10 percent increase from threshold value, the switching occurs slightly faster under uniform case. The expla-

nation of these distinction is that the strength of the threshold values for uniform fields are quite high and

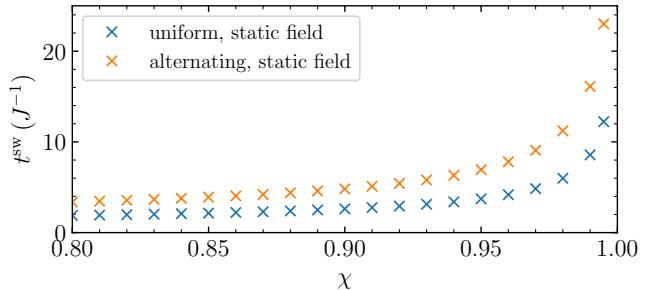


FIG. 13. Switching time comparison under uniform and alternating fields.

no additional support from effective fields are provided. However, under alternating fields, the sublattice magnetizations benefit from effective fields and hence only initial external energy for small canting is needed. As a result, switching occurs rather late but the overall dependence on anisotropy is the same.

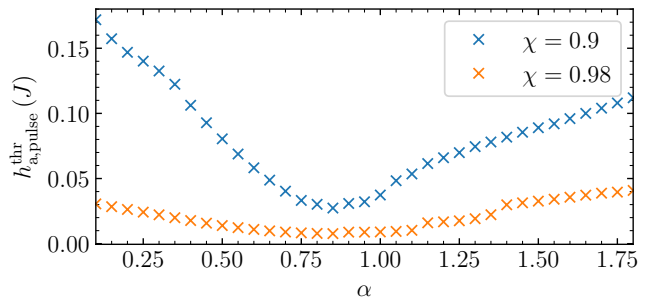


FIG. 14. Switching time dependence on normalization constant. Other optimum parameters of the pulse are $\tau = 10 J^{-1}$ and $\phi_0 = \pi/3$.

The switching facilitates from time-dependent external fields at resonance with the spin gap, although the actual pulse duration is very short. To capture the full period of oscillations, we shifted the THz pulse from the time $t = 0$ by $\tau = 30 J^{-1}$ as it was mentioned in 3D case. So, here also we analyze the dynamics of sublattice magnetization in square lattice under the Gaussian pulse, given by (8). The spin gaps in (15) are calculated for square lattice with nearest neighbor interactions with respect to easy-axis anisotropy parameter. Fig. 14 shows threshold field dependence on frequency renormalization constant. As expected, the optimal switching occurs at $\alpha \approx 0.85$ with minimum threshold field. Lastly, Fig. 15 and Fig. 16 show the effect of initial phase and pulse duration on the threshold field, respectively. The results perform a justification for the cases in 3D.

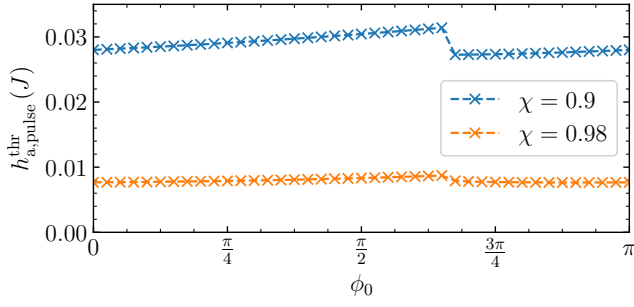


FIG. 15. Switching time dependence on initial phase

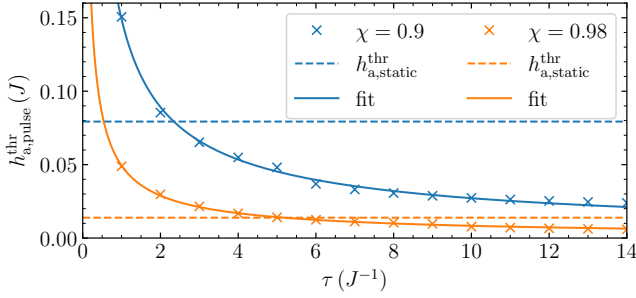


FIG. 16. Switching time dependence on pulse duration. The parameters in the pulse are $\alpha = 0.85$ and $\phi_0 = \pi/3$. Dashed horizontal lines correspond to the threshold values for alternating static magnetic field with $h_{a,static}^{thr} = 0.079 J$ and $h_{a,static}^{thr} = 0.0138 J$ for $\chi = 0.9$ and $\chi = 0.98$, respectively. The fits (solid lines) are done by power laws $h_{a,pulse}^{thr} = a\tau^b$ with parameters $a = 0.148 J^{b+1}$, $b = -0.739$ for $\chi = 0.9$ and $a = 0.049 J^{b+1}$, $b = -0.772$ for $\chi = 0.98$.